

# Surface modified ZnO nanoparticles: structure, photophysics, and its optoelectronic application

Punita Singh · O. P. Sinha · Ritu Srivastava ·  
A. K. Srivastava · Som V. Thomas · K. N. Sood ·  
M. N. Kamalasanan

Received: 15 January 2013 / Accepted: 27 May 2013 / Published online: 13 June 2013  
© Springer Science+Business Media Dordrecht 2013

**Abstract** Nanostructured ZnO has been synthesized by wet chemical route. Poly(vinylpyrrolidone) is used for stabilization and surface passivation of synthesized nanoparticles, thus tailoring the growth of ZnO at nanoscale. Structural characterization using X-ray diffraction, scanning electron microscopy, high-resolution transmission electron microscopy and Fourier transformed infrared spectroscopy of the synthesized nanoparticles confirm the evolution of nanocrystalline ZnO prevailing in hexagonal wurtzite phase. UV–Vis and photoluminescence spectroscopy studies show blue shift phenomenon in the synthesized nanoparticle in contrast to the bulk ZnO furnishing evidence in support of quantum size effect. The nanocomposites of ZnO and poly [9,9-dioctylfluorenyl-2,7-diyl] are prepared and characterized to investigate its luminescent and spectral emission effects. The nanocomposites are then incorporated in light-emitting diodes, and influence of ZnO on the device performance has been explored via

electroluminescence, current density evaluation, and corresponding CIE coordinates calculation.

**Keywords** Photoluminescence · Nanocomposites · Electroluminescence

## Introduction

Organic light-emitting diodes (OLEDs) have attracted considerable attention as a potential next generation technology for flat panel displays, solid-state lighting, and flexible electronic devices (Tang and Van Slyke 1987; Xing et al. 2012) etc. It relies on multilayer architecture obtained under high-vacuum conditions. For commercial success, extensive research efforts are put forth to improve the efficiency and stability of the devices particularly in solution-processable polymeric materials in polymeric OLEDs (PLEDs). Polymer-based optoelectronics has been a subject of research in past few decades (Lee et al. 2012; Shaw-Stewart et al. 2012), and white PLEDs (Zhu et al. 2012; Lee et al. 2010) have generated significant interest for solid-state lighting applications, due to the potential savings in both costs and energy consumption. Besides the device optimization, a strong reduction in production costs is urged in order to make organic lighting competitive with the current technologies. Hence, focus is emphasized on nanocrystal-polymer composites owing to abundant progress in the hybrid organic–inorganic light-emitting diodes (HyLEDs), demonstrating the

---

P. Singh · R. Srivastava (✉) · M. N. Kamalasanan  
Centre for Organic Electronics, Physics of Energy  
Harvesting Division, CSIR-National Physical Laboratory,  
New Delhi 110012, India  
e-mail: ritu@mail.nplindia.org

O. P. Sinha · S. V. Thomas  
Amity Institute of Nanotechnology, Amity University,  
Noida 201303, Uttar Pradesh, India

A. K. Srivastava · K. N. Sood  
Electron and Ion Microscopy, CSIR-National Physical  
Laboratory, New Delhi 110012, India

possibility to prepare air-stable electroluminescent devices. The synthesized nanoparticles can be incorporated into polymer host system to explore the appealing possibilities of synergetic properties of both the components resulting into combining the natural advantages from both organic as well as inorganic materials into one system. In HyLEDs, the high-electron mobility of the inorganic phase compared with that of organic materials stabilizes the limited electron mobility (Antoniadis et al. 1994) in organic materials and help to balance the charge transport. Moreover, colloiddally synthesized (Kim et al. 2008) inorganic semiconductor quantum dots (QDs) are being widely used for their narrow spectral emission, and luminance, ease of solution deposition across large area. Metal oxide ZnO (Klingshirn et al. 2010) is a semiconductor having wide bandgap, with strong electron–hole binding energy of 60 meV. Similarly, it is an attractive material for optical applications ranging from white light illumination to lasers in the near UV. It spans a wide range of applications from luminescent devices and chemical sensors, to electrical, acoustic, and solar cells. It also provides favorable properties like good mechanical and compositional stability, transparency, good electrical conductivity etc. In present studies, we have synthesized nanoscale ZnO and studied the influence of temperature treatment to these freshly synthesized nanoparticles and assessed the morphology and emission properties along with the effect on the device performance.

## Experimental

### Material synthesis

For synthesis of ZnO, a solution of zinc acetate  $(\text{CH}_3\text{COO})_2\text{Zn}\cdot 2\text{H}_2\text{O}$  (SRL, India) in 2-propanol (0.5 mM) were prepared (Guo et al. 2000) under vigorous stirring along with mild heating followed by chilling to 0 °C. 0.075 mol of Poly(vinylpyrrolidone) (PVP) (Aldrich, MW 40,000; 3.0 g) were then introduced in the above solution as a capping molecule under vigorous stirring at room temperature. The mixtures were then hydrolyzed by addition of 50 ml of 0.002 M NaOH solution in 2-propanol and subjected to an ultrasonic bath for 2 h. Thus, colloidal suspensions of ZnO were obtained. The nanoparticles were then extracted using centrifuge (10,000 rpm) and

dried under vacuum in two aliquots, at room temperature (40 °C) for several hours and at 80 °C for 1 h. The ZnO nanoparticles were then formulated in thin film form with a fluorescent blue emitter, poly[9,9-dioctylfluorenyl-2,7-diyl] (PFO) and assembled in PLEDs to observe its consequence.

### Nanocomposite preparation

ZnO nanoparticles were dispersed (by weight percent) in a blend (1:1) of chloroform and chlorobenzene. The nanocomposites were prepared by adding PFO (American Dye Source) (8 mg/ml) into the ZnO dispersion and subjected to an ultrasonic bath. Homogeneous yellow hybrid precursors were thus obtained emitting blue light upon exposure to UV rays. These nanocomposites were used as emissive layer (EML) in OLEDs

### Device fabrication

The OLEDs were fabricated on indium–tin–oxide (ITO) coated glass substrates having a sheet resistance of 20  $\Omega$ /square and a thickness of 120 nm, which were patterned and then cleaned using deionized water, acetone, trichloroethylene, and isopropyl alcohol sequentially for 20 min each using an ultrasonic bath and dried in vacuum oven. Prior to organic film deposition, ITO surfaces were treated with oxygen plasma for 5 min to increase its work function. PEDOT: PSS (Aldrich) films (HIL) were spin coated (~50-nm thick) on the cleaned and patterned ITO substrates. The films were then cured at 120 °C in vacuum for ~1 h. The PFO:ZnO hybrid precursors (50–55 nm) were then spin coated with a speed of 2,000 rpm for 2 min on substrates followed by vacuum annealing at 150 °C for ~2 h to remove the organic fraction and improve the connectivity and crystallinity at nanoscale. Thicknesses of the deposited layers were measured by ellipsometry. Finally, Al electrodes were deposited by vacuum thermal evaporation of thickness 200 nm under a vacuum of  $1 \times 10^{-6}$  Torr. Due care was taken to prevent the attack of moisture throughout the processes. Following devices were fabricated:

ITO/PEDOT: PSS/Pristine PFO/Al  
ITO/PEDOT: PSS/PFO: 11 % ZnO(40 °C)/Al  
ITO/PEDOT: PSS/PFO: 11 % ZnO(80 °C)/Al

The complete devices were finally annealed at 100 °C in vacuum for 5 min before being characterized.

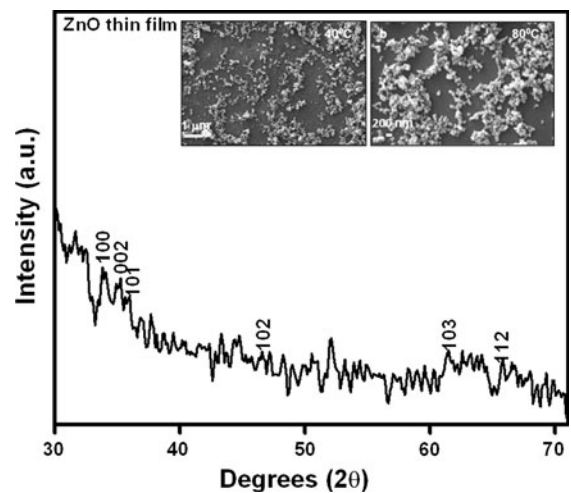
Four pixels, each of active area of  $0.16 \text{ cm}^2$  are defined per substrate, which were used to assess the reproducibility of the device performance.

In order to probe the crystalline structure of ZnO nanoparticles, X-ray diffraction of thin films were performed with Bruker AXS D8 Advance Diffractometer at room temperature using  $\text{CuK}\alpha$  radiation ( $\lambda = 1.5405 \text{ \AA}$ ). The surface morphological characteristics of ZnO thin films (drop-cast) were examined using a LEO 440 scanning electron microscope (SEM). Fourier Transform Infrared (FT-IR) spectra of the ZnO nanoparticles were recorded in KBr pellets (13 mm diameter) with Perkin Elmer FT-IR spectrometer in the wavenumber range of  $4,000\text{--}400/\text{cm}$  at room temperature. Atomic force microscopy (AFM) experiments were performed on  $10 \times 10 \mu\text{m}$  surface area using NT-MDT (Solverpro) operating in tapping mode. High-resolution Transmission electron microscopy (HR-TEM) images of the nanoparticles were recorded on a 300 kV HR-TEM, (FEI Tecnai G2 F30 STWIN) by dispensing few microliters of ZnO dispersion on carbon coated copper grid of 3.05 mm diameter. Optical absorptions were recorded in  $200\text{--}800 \text{ nm}$  wavelength range in a UV-2401 PC SHIMADZU, Japan, and photoluminescence (PL) spectroscopy was done on FL-1039 HORIBA JOBIN-YVON, USA. Current-density versus voltage (J-V) curves of the devices were recorded in air at room temperature using Keithley 2612A Dual Source Meter. To have better qualities of the interface between each successive layer, the quality of each layer was tested using HIOKI 3520-50 LCR High tester (data not shown). Electroluminescence spectra of the devices were obtained using Ocean Optics HR2000CG-UV-NIR spectrophotometer.

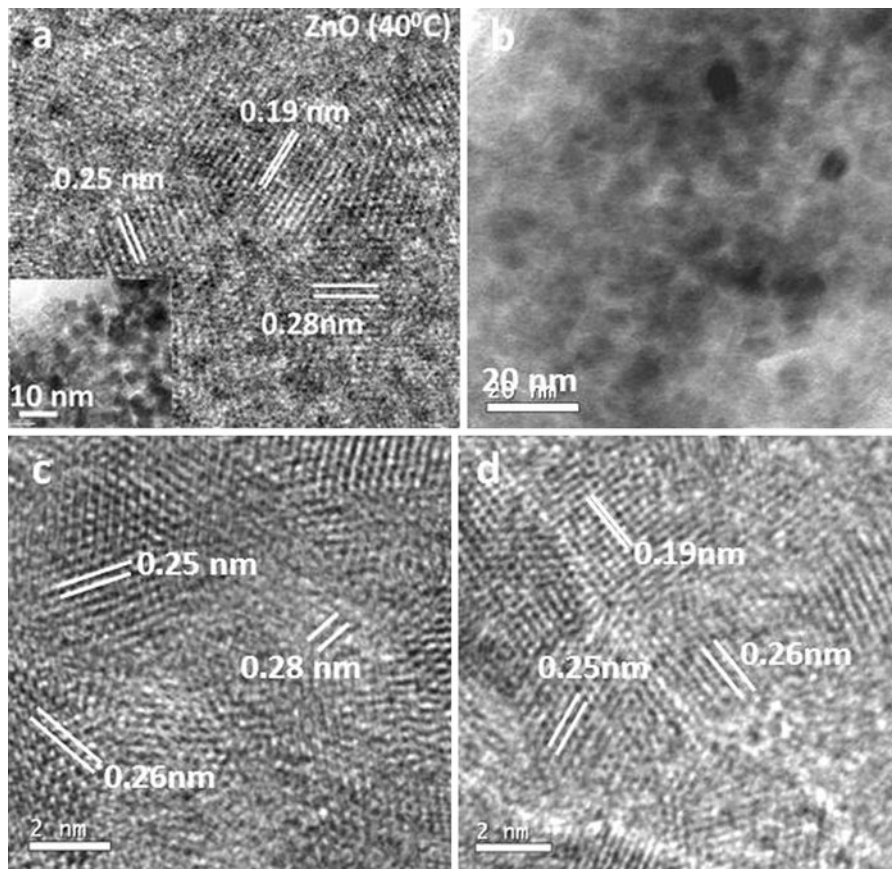
## Results and discussion

Figure 1 shows the X-ray diffractograms of the ZnO nanoparticle. The films reveal several peaks characteristic of the hexagonal wurtzite phase of ZnO. The data are consistent with the standard powder diffraction pattern of hexagonal wurtzite phase (JCPDS Card No. 80-0075). The peaks observed at  $d = 0.28, 0.26, 0.25, 0.19, 0.15,$  and  $0.14 \text{ nm}$  (Fig. 1) match the  $d$ -values of hexagonal wurtzite structure of ZnO in accordance to the (100), (002), (101), (102), (103), and (112) planes of this phase (Caglar et al. 2006; Sui et al. 2006). However,

the peaks are predicted of comparatively lower intensities probably due to very fine particle size. The scanning electron micrographs (insets in Fig. 1) of ZnO nanoparticles thin film elucidate fine grain growth with uniform microstructure throughout the film.  $40 \text{ }^\circ\text{C}$ , sample (inset a, Fig. 1) reveal fine grained surface morphology. However, annealing at  $80 \text{ }^\circ\text{C}$  initiates growth and development of prominent spherical inter-linked grains (inset b, Fig. 1). A detailed microstructural characterization using high-resolution transmission electron microscopy (HR-TEM) on ZnO nanopowder particles (Fig. 2a–d) elucidated several interesting features in terms of the size and shape of the particles and lattice scale arrangement of different atomic planes in the crystal structure. In general, it was noted that the microstructure of ZnO powders prepared at  $40 \text{ }^\circ\text{C}$  (Fig. 2a) was ultra-fine with individual particles of size ranging between 2 and 5 nm. The morphology of individual particles is random having sharp edges with well-defined facets coexisting with large fraction of the grain boundaries and the amorphous structure (inset in Fig. 2a). Lattice scale imaging performed on these nanoparticles revealed the presence of several crystallographic planes of hexagonal crystal structure of ZnO (Reference JCPDS card no. 80-0075, Hexagonal space group:  $P6_3mc$ , lattice constants:  $a = 0.325 \text{ nm}$  and  $c = 0.521 \text{ nm}$ ). As an illustrative example, a set of crystallographic planes with interplanar spacing of  $0.28 \text{ nm}$  (hkl:100),  $0.25 \text{ nm}$  (hkl:101), and  $0.19 \text{ nm}$  (hkl:102) of a hexagonal crystal structure (Fig. 2a). The



**Fig. 1** XRD pattern of ZnO thin film (drop cast): inset shows scanning electron micrographs of ZnO nanoparticles cured at **a**  $40 \text{ }^\circ\text{C}$  and **b**  $80 \text{ }^\circ\text{C}$



**Fig. 2** High-resolution transmission electron micrographs of ZnO showing microstructure of ZnO cured at **a** 40 °C (lattice scale image); inset shows crystalline morphology at low

magnification, **b-d** shows ZnO cured at 80 °C displaying **b** morphology and **c, d** lattice scale images

size of the nanoparticles observed for the case of ZnO synthesized at higher temperature (80 °C) was albeit on higher range between 3 to 8 nm, but their external contour was more or less same as in case of ZnO prepared at 40 °C (Fig. 2b). The corresponding lattice scale images (Fig. 2c, d) exhibited the presence of important planes; 0.28 nm (hkl:100), 0.26 nm (hkl:002), 0.25 nm (hkl:101), and 0.19 nm (hkl:102), of ZnO hexagonal crystal structure. It is important to note that the crystallinity in the annealed sample is quite improved with the sharp appearance of the atomic planes within the individual nanocrystals. FTIR analysis was performed in order to elucidate the possible coordination of ZnO nanoparticle with the capping molecule PVP. FTIR (Fig. 3) display intense peaks at 1,043 and 1,670/cm (narrow) representing C–N and C=O functional groups of PVP, respectively, which seems to be shifted toward high wavenumber in contrast

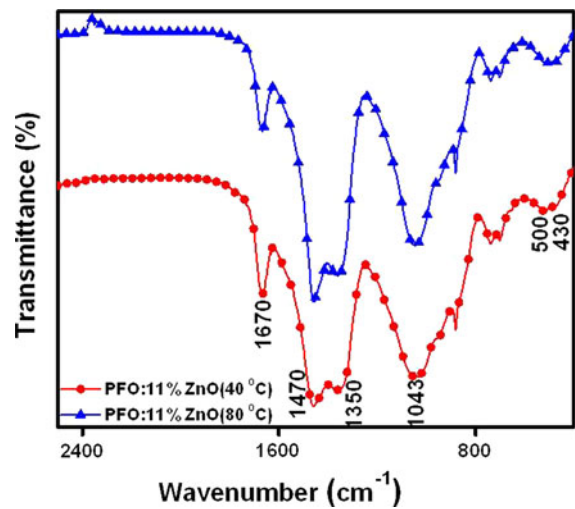


**Fig. 3** FTIR spectra of ZnO nanoparticles in the range of 2,500–400/cm

to the bonds in pristine PVP (Zhang et al. 2010; Chahal et al. 2011). It is assumed that these shifts arise owing to partial donation of the lone pair of electrons from N and O atoms to the vacant orbitals of  $Zn^{2+}$ , thus, leading to the formation of coordination bonds between pyrrolidone ring and ZnO. Bands at 1,470 and 1,350/cm corresponds to the vibration in pyrrolidone ring (Zhang et al. 2010). Two weak bands were observed at about 500 and 430/cm, which probably corresponds to oxygen deficiency and/or oxygen vacancy defect complex and Zn–O stretching bond in ZnO, respectively (Xiong et al. 2006). UV–Vis absorption spectra of ZnO (Guo et al. 2000; Son et al. 2012) nanoparticles dispersed in a blend of chloroform and chlorobenzene (1:1) are shown in inset in Fig. 4. A strong exciton absorption feature appears at 270 nm owing to the relatively large exciton binding energy (60 meV in bulk ZnO), and the significant blue shift of this feature relative to the bulk exciton absorption (373 nm). This confinement effect is consistent with the small size of the synthesized ZnO nanoparticles using PVP capping. Upon annealing the nanoparticles at 80 °C, a weak hump of 340 nm is found to be associated with the peak at 270 nm (inset in Fig. 4). Probably, this indicates broader size distribution of the synthesized ZnO nanoparticles. Additionally, absorbance curve bends in a tail running in the entire visible region. The photoluminescence (PL) spectra (Fig. 4) emerged as vital studies here, owing to gain specifics of the PL emission in the synthesized nanocrystalline ZnO. The PL process is closely related to the

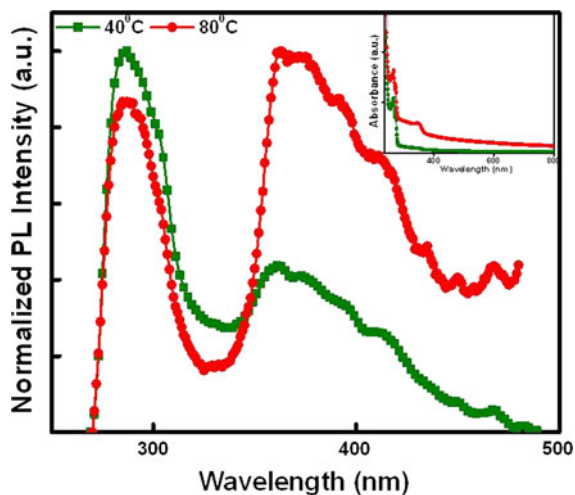
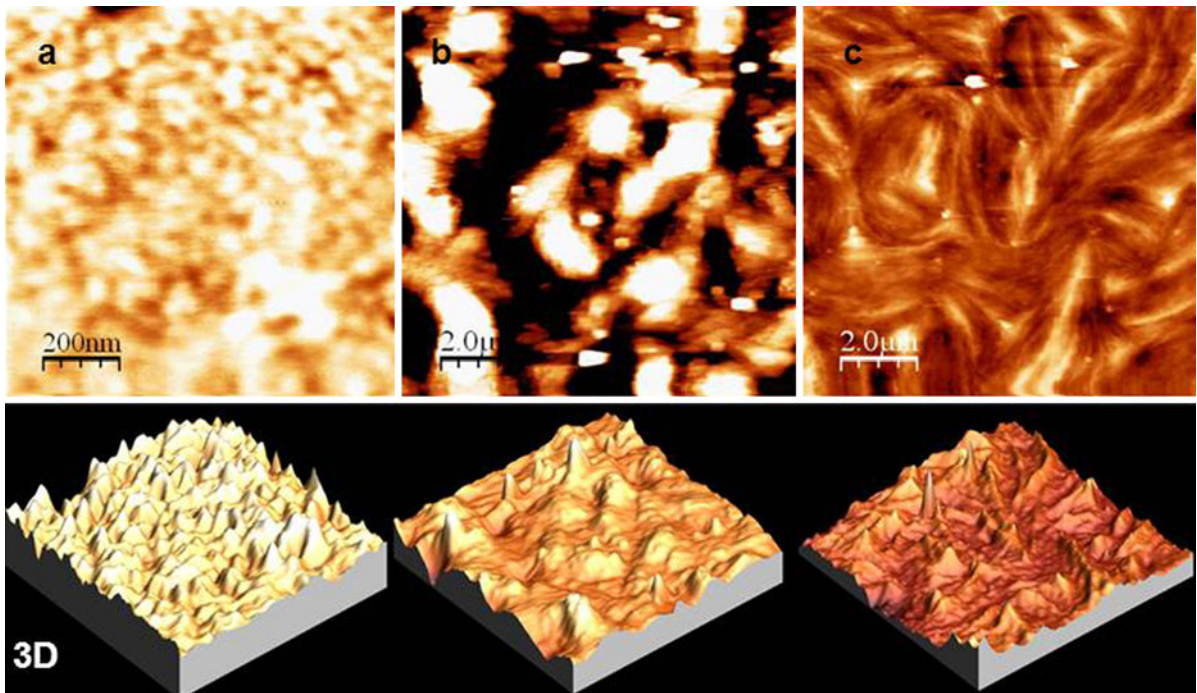


**Fig. 4** Normalized photoluminescence (PL) spectra of ZnO nanoparticles dispersed in a blend of chloroform and chlorobenzene (1:1); inset shows normalized UV–Vis absorption

surface stoichiometry and band gap transitions of the nanomaterial. Emission in the visible region entails the formation of various animated energy levels within the forbidden gap due to a large number of surface “broken” or dangling bonds and defect centers in their structure (Xiong et al. 2006; Hai-Bo et al. 2007). Here, the spectrum of the ZnO nanoparticles upon excitation at 260 nm demonstrate an outstanding narrow emission at  $\sim 285$  nm followed by a broad emission centered at 360 nm, the tail of which is extending in the visible region. Upon annealing the nanocrystalline ZnO at 80 °C for 1 h, the peak at 285 nm decreases in intensity whereas the 360 nm peak dominates with a broad tail in the visible region.

#### Characterization of nanocomposites

To obtain the relevant surface parameters of the films using AFM, the nanocomposites of PFO:ZnO were spin coated on glass slides at a speed of 2,000 rpm for 2 min followed by vacuum annealing at 150 °C for  $\sim 2$  h to follow the analogous pattern of film assembly used in the device. The rms roughness demonstrates the increasing pattern for PFO and its nanocomposite film (Fig. 5). For pristine PFO, the rms roughness observed was 2.53 nm (Fig. 5a). Addition of ZnO (cured at 40 °C) increases the roughness to 9.24 nm, (Fig. 5b) renders the development of very fine particles. Here, aggregation or masses lead to increase in domain size. As the annealing temperature is enhanced to 80 °C, the roughness increases to 11.34 nm inducing evolution of nano-scaled crystallinity (Fig. 5c). Here, the nanoparticle seems to be coarse, distributed uniformly throughout the polymer matrix. 3-D images of pristine PFO and its hybrid shown in Fig. 5 elucidate surface topography as a function of ZnO concentration and the impact of annealing treatment. Photophysical studies on pristine PFO and its hybrids with ZnO (Fig. 6) show variation in their solution and thin film forms. In solution phase, an intense absorption peak ( $\lambda_{\max}$ ) (inset in Fig. 6a) of pristine PFO is observed at 389 nm (Kulkarni and Jenekhe 2003, Chen et al. 2005). Addition of 40 °C and 80 °C annealed ZnO (inset in Fig. 6a) does not show any shift in the absorption maxima of PFO. However, the intensity of absorption intensifies with its addition in both cases. The absorption spectrum reveals a red shift in the  $\lambda_{\max}$  position on moving from solution phase to thin film forms. Moreover, thin film spectrum (inset in



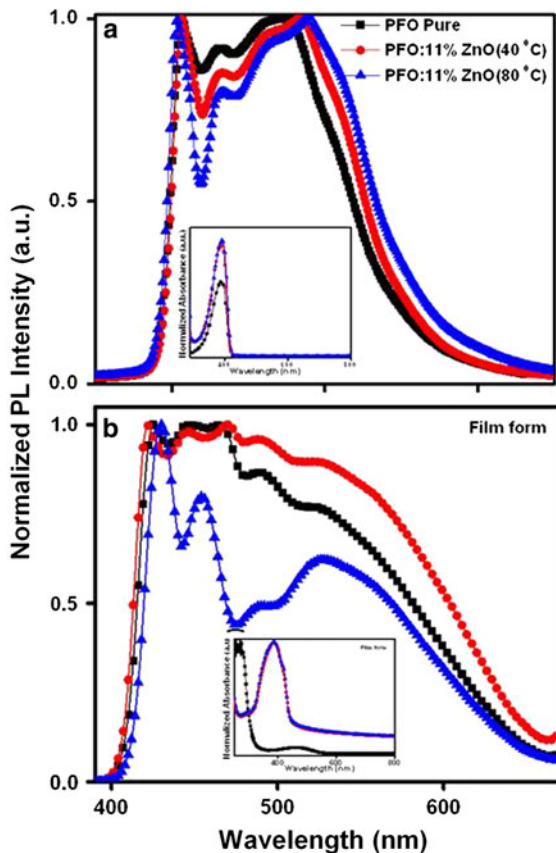
**Fig. 5** AFM images (surface plots) of (a) pristine PFO, (b) PFO: 11 % ZnO (40 °C), and (c) PFO: 11 % ZnO (80 °C); corresponding three-dimensional images shown below

Fig. 6b) is broader in comparison to its solution phase and the variation in the intensity upon addition of ZnO is more pronounced. A broad hump in the high energy at about 285 nm is observed in the both PFO:ZnO hybrids whereas a shoulder at 418 nm is observed in PFO: ZnO (80 °C) alone. For PL, several peaks of high to medium intensities are clearly perceptible for pristine PFO (in solution phase) (Fig. 6a) at about 406 (sharp), 430 (merged), and 470 (broad) nm. For PFO: 11 % ZnO (40 °C) hybrid, peaks are more noticeable (color purity) and are observed in similar nanometer range along with a peak at 470 nm separating into 460 and 480 nm and is slightly red shifted. Similar spectral emission is observed in PFO: 11 % ZnO (80 °C) hybrid with the peak at 406 nm becoming more prominent besides, peaks are red shifted by few nm. As PFO and their hybrids were deposited in thin film forms (Fig. 6b) followed by annealing at 150 °C for 2 h, the PL emission for pristine PFO at 406 nm is found to red shift by 20 nm, along with peaks at 440 and 465 nm almost merging with equal intensity. A peak of low intensity at 490 nm is also observed with a broad shoulder in red region at about 525 nm. PFO with 11 % ZnO (40 °C) (Fig. 6b) shows 406 nm peak red shifted by 14 nm and

emerging at 420 nm, along with peaks at 445, 470 nm (almost merging) of equal intensity. A peak of intensity higher than the pristine PFO at 490 nm is also observed with a broad shoulder in red region at 525 nm. The PFO with 11 % ZnO (40 °C) is intensified in the entire spectral region and is broadening and covering almost entire visible region of the spectrum. PFO with 11 % ZnO (80 °C) hybrid shows red shift of 406 nm peak by 24 nm, evolving at 430 nm along with prominent peak at 450 nm followed by a peak at 490 and 525 nm similar to the other two films, but are of lower intensity (Fig. 6b).

#### *Characterization of device*

Prototype OLED devices were fabricated using pristine PFO and their hybrids with ZnO as EML, and the current density versus voltage curve (Fig. 7a) of the fabricated device was obtained. The characteristics of the current density against the applied voltage reveal excellent diode behavior displaying the driving voltage for the device with pristine PFO to be 4–5 V. The device with PFO: ZnO hybrids show decrease in the turn-on voltage to about 3–4 V. The J–V curve specifies that the current passing through hybrid



**Fig. 6** Photoluminescence spectra (PL) of the nanocomposites in (a) solution phase and (b) thin film form; inset shows UV–Vis absorption of the nanocomposites in solution and thin film forms, respectively

device in low-voltage region (below 4 V) is higher than the pure device probably due to excess charge carrier generation at low voltage. Above 4 V current gain appears to be lower than in the pristine PFO device suggesting better charge recombination efficiency in the PFO:ZnO hybrid devices. Low current in these hybrids is expected to improve the device lifetime. Besides, in PFO: 11 % ZnO (80 °C) device, current propagation is still lower than the other two devices and its performance is stable up to high voltages (large operational window/stability). It is possible that the annealing of ZnO at 80 °C renders better dispersion of the nanoparticles, enhanced crystallization at nano scale, and improves charge injection at the interface. The electroluminescence (Fig. 7b–d) of the fabricated devices was assessed in

three different devices. For the device with pristine PFO, electroluminescence (EL) emission (at 7 V) (Fig. 7b) is observed at 435, 460, 495, and 525 nm, showing spectral stability with amplified voltage. However, the peaks resolve better with enhancement in voltage. The CIE coordinates (Fig. 7e) calculated for the Pristine PFO is (0.28, 0.33) quite close to pure white-light emission of (0.33, 0.33). Device with PFO: 11 % ZnO (40 °C) shows narrow emission (overall spectral width) peaking at 430, 455, and 490 nm along with a tail in red region. The EL emission is slightly blue shifted and the spectral emission in the blue region is more pronounced in comparison to the pristine polymer. It is to be noted that the peak for blue emission is far more pronounced than its green spectral emission as well as the broadness of the total emission range is increasing with prominence of the peak in a blue region and a tail in the red region. Besides enhanced broadness, the pronounced spectral emission in blue region in conjunction with a tail in red region leads to the generation of white light. Consequently, the CIE coordinates calculated slightly tilted toward blue region at (0.29, 0.28). The EL emission for PFO: 11 % ZnO (80 °C) hybrid device appears at 430, 455, and 485 nm with a shoulder at 506 nm revealing blue shift in contrast to pristine PFO. It appears that the peak for green emission is more prominent than its blue spectral emission as well as the broadness of the total emission range (overall spectral width) seems to cover the entire visible region. Here, with increased green emission and broadening of spectral emission, white light is emitted. The CIE coordinates calculated in PFO:11 % ZnO (80 °C) is observed at (0.28, 0.30) inclined toward green, producing white light. It is to be noted that the charge transport in polymers follow hopping phenomenon. Stabilization of EL peaks in PFO doped ZnO, is probably due to the creation of additional hopping sites leading to shortening of hopping distance facilitating transport properties (Rao et al. 2009). Simultaneously, enhanced crystallization or roughness (low amorphosity) improves dispersion of the ZnO in the polymer matrix (also indicated by AFM and TEM studies) modifying morphology of the polymer film PFO. Consequently, it increases the interfacial area between the EML film and the Al cathode, and thus accelerate electron injection refining radiative recombination (Rao et al. 2009).

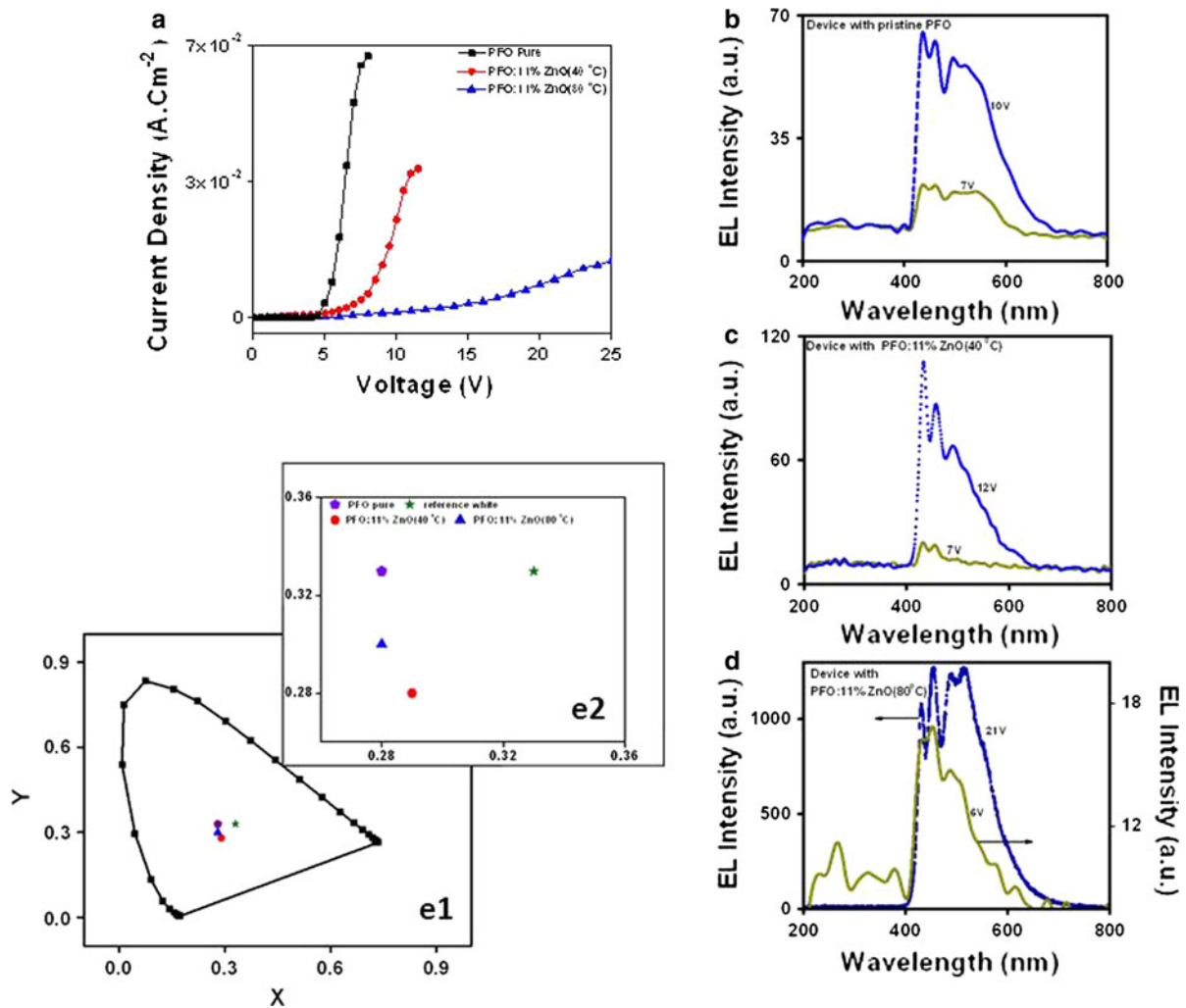


**Fig. 7** a Current density versus voltage curve (J–V) of the fabricated device using PFO:ZnO nanocomposites; EL spectra of the devices recorded at room temperature using (b) pristine

PFO, (c) PFO: 11 % ZnO (40 °C) and (d) PFO: 11 % ZnO (80 °C); (e1, e2) shows corresponding CIE coordinates

## Conclusion

Zinc oxide was synthesized by wet chemical method. Structural and microstructural examinations ascertained evolution of ultrafine particles with narrow size distribution ensuing hexagonal wurtzite phase. Curing of particles at different temperatures, points to change in growth morphology revealing variation in spectral emission most likely due to enhanced defect emission. High-temperature treatments demonstrate better nanocrystalline ZnO, well dispersed in PFO. The nanocomposites (PFO:ZnO) show enhanced optical absorption while PL studies does not show significant change except for PFO: 11 % ZnO (80 °C) film.

Fabricated hybrid device show improved EL and turn-on voltage along with enhanced stability (can sustain high voltage), which is a direct consequence of the modified surface morphology noticeable through curing treatments. The pristine PFO device gives white emission and by addition of ZnO white emission sustains with enhanced stability.

**Acknowledgments** The authors thank the Director, National Physical Laboratory, New Delhi, for his constant support and for providing lab facilities. Authors, Dr. Punita Singh thanks the Council of Scientific and Industrial research for the award of Senior Research Associateship, and Dr. O.P. Sinha is highly thankful to the Department of Science and Technology, Govt. of India, for the financial support.



## References

- Antoniadis H, Abkowitz MA, Hsieh BR (1994) Carrier deep-trapping mobility-lifetime products in poly(p-phenylene vinylene). *Appl Phys Lett* 65:2030–2032
- Caglar M, Caglar Y, Ilcan S (2006) The determination of the thickness and optical constants of the ZnO crystalline thin film by using envelope method. *Optoelectron J Adv Mater* 8:1410–1413
- Chahal RP, Mahendia S, Tomar AK, Kumar S (2011) Effect of ultraviolet irradiation on the optical and structural characteristics of in situ prepared PVP-Ag nanocomposites. *Digest J Nanomater and Biostr* 6:299–306
- Chen SH, Su AC, Su CH (2005) Crystalline Forms and Emission Behavior of Poly(9,9-di-*n*-octyl-2,7-fluorene). *Macromolecules* 38:379–385
- Guo L, Yang S, Yang C, Yu P, Wang J, Ge W, Wong GKL (2000) Synthesis and characterization of poly(vinylpyrrolidone)-modified zinc oxide nanoparticles. *Chem Mater* 12:2268–2274
- Hai-Bo F, Shao-yan Y, Pan-feng Z, Hong-yuan W, Xiang-lin L, Chun-mei J, Qin-sheng Z, Yong-hai C, Zhan-guo W (2007) Investigation of oxygen vacancy and interstitial oxygen defects in ZnO films by photoluminescence and X-ray photoelectron spectroscopy. *J Electron Spectrosc* 24:2108–2111
- Kim LA, Anikeeva PO, Coe-Sullivan SA, Steckel JS, Bawendi MG, Bulovic V (2008) Contact printing of quantum dot light-emitting devices. *Nano Lett* 8:4513–4517
- Klingshirn C, Fallert J, Zhou H, Sartor J, Thiele C, Maier-Flaig F, Schneider D, Kalt H (2010) 65 years of ZnO research—old and very recent results. *Phys Stat Sol B* 247:1424–1447
- Kulkarni AP, Jenekhe SA (2003) Blue light-emitting diodes with good spectral stability based on blends of poly(9,9-dioctylfluorene): interplay between morphology, photophysics, and device performance. *Macromolecules* 36:5285–5296
- Lee BR, Kim J, Kang D, Lee DW, Ko S, Lee HJ, Lee C, Kim JY, Shin HS, Song MH (2012) Highly efficient polymer light-emitting diodes using graphene oxide as a hole transport layer. *ACS Nano* 6:2984–2991
- Po-I Lee, Hsu SLC, Lin P (2010) White-light-emitting diodes from single polymer systems based on polyfluorene copolymers with quinoxaline derivatives. *Macromolecules* 43:8051–8057
- Rao MVM, Su YK, Huang TS, Yeh CH, Tu ML (2009) Electroluminescent characteristics of DBPPV–ZnO nanocomposite polymer light emitting devices. *Nanoscale Res Lett* 4:485–490
- Shaw-Stewart JRH, Lippert TK, Nagel M, Nüesch FA, Wokaun A (2012) Sequential printing by laser-induced forward transfer to fabricate a polymer light-emitting diode pixel. *ACS Appl Mater Interfaces* 4:3535–3541
- Son DI, Kwon BW, Park DH, Seo W, Yi Y, Angadi B, Lee C, Choi WK (2012) Emissive ZnO–graphene quantum dots for white-light-emitting diodes. *Nature Nanotech* 7:465–471
- Sui X, Liu Y, Shao C, Liu Y, Xu C (2006) Structural and photoluminescent properties of ZnO hexagonal nanoprisms synthesized by microemulsion with polyvinyl pyrrolidone served as surfactant and passivant. *Chem Phys Lett* 424:340–344
- Tang CW, Van Slyke SA (1987) Organic electroluminescent diodes. *Appl Phys Lett* 51:913–915
- Xing X, Zhang L, Liu R, Li S, Qu B, Chen Z, Sun W, Xiao L, Gong Q (2012) A deep-blue emitter with electron transporting property to improve charge balance for organic light-emitting device. *ACS Appl Mater Interfaces* 4:2877–2880
- Xiong G, Pal U, Serrano JG, Ucer KB, Williams RT (2006) Photoluminescence and FTIR study of ZnO nanoparticles: the impurity and defect perspective. *Phys Stat Sol (C)* 3:3577–3581
- Zhang Y, Xu J, Xu P, Zhu Y, Chen X, Yu W (2010) Decoration of ZnO nanowires with Pt nanoparticles and their improved gas sensing and photocatalytic performance. *Nanotechnology* 21:285501–285507
- Zhu M, Zou J, Hu S, Li C, Yang C, Wu H, Qin J, Cao Y (2012) Highly efficient single-layer white polymer light-emitting devices employing triphenylamine-based iridium dendritic complexes as orange emissive component. *J Mater Chem* 22:361–366